



# Passive Diffusion vs Active pH-Dependent Encapsulation of Tyrosine Kinase Inhibitors Vandetanib and Lenvatinib into Folate-Targeted Ferritin Delivery System

This article was published in the following Dove Press journal:  
*International Journal of Nanomedicine*

Zuzana Skubalova <sup>1,2</sup>

Simona Rex <sup>1,2</sup>

Martina Sukupova <sup>1</sup>


Martin Zahalka<sup>1</sup>

Petr Skladal<sup>3</sup>

Jan Pribyl <sup>3</sup>

Hana Michalkova <sup>1,2</sup>

Akila Weerasekera<sup>4</sup>

Vojtech Adam <sup>1,2</sup>

Zbynek Heger <sup>1,2</sup>

<sup>1</sup>Department of Chemistry and Biochemistry, Mendel University in Brno, Brno, Czech Republic; <sup>2</sup>Central European Institute of Technology, Brno University of Technology, Brno, Czech Republic; <sup>3</sup>Central European Institute of Technology, Masaryk University, Brno, Czech Republic; <sup>4</sup>Athinoula A. Martinos Center for Biomedical Imaging, Massachusetts General Hospital, Harvard Medical School, Charlestown, MA, USA

**Introduction:** The present study reports on examination of the effects of encapsulating the tyrosine kinase inhibitors (TKIs) vandetanib and lenvatinib into a biomacromolecular ferritin-based delivery system.

**Methods:** The encapsulation of TKIs was performed via two strategies: i) using an active reversible pH-dependent reassembly of ferritin's quaternary structure and ii) passive loading of hydrophobic TKIs through the hydrophobic channels at the junctions of ferritin subunits. After encapsulation, ferritins were surface-functionalized with folic acid promoting active-targeting capabilities.

**Results:** The physico-chemical and nanomechanical analyses revealed that despite the comparable encapsulation efficiencies of both protocols, the active loading affects stability and rigidity of ferritins, plausibly due to their imperfect reassembly. Biological experiments with hormone-responsive breast cancer cells (T47-D and MCF-7) confirmed the cytotoxicity of encapsulated and folate-targeted TKIs to folate-receptor positive cancer cells, but only limited cytotoxic effects to healthy breast epithelium. Importantly, the long-term cytotoxic experiments revealed that compared to the pH-dependent encapsulation, the passively-loaded TKIs exert markedly higher anticancer activity, most likely due to undesired influence of harsh acidic environment used for the pH-dependent encapsulation on the TKIs' structural and functional properties.

**Conclusion:** Since the passive loading does not require a reassembly step for which acids are needed, the presented investigation serves as a solid basis for future studies focused on encapsulation of small hydrophobic molecules.

**Keywords:** drug delivery, nanomedicine, lenvatinib, vandetanib

## Introduction

Cancer chemotherapeutics can be considered as one of the major medical advances of the last few decades. However, chemotherapeutic agents have a narrow therapeutic index, and the outcomes are sometimes palliative as well as unpredictable.<sup>1</sup> Therefore, targeted therapy that aims at delivering drugs to cancer cells through specific surface molecules or the tissue microenvironment is the golden grail of contemporary cancer chemotherapy.<sup>2</sup>

Among the most promising candidates acquiring precise targeting are small molecule tyrosine kinase inhibitors (TKIs). These belong to the most promising modalities able to

Correspondence: Zbynek Heger  
Department of Chemistry and Biochemistry, Mendel University in Brno, Zemedelska 1, Brno CZ-613 00, Czech Republic  
Tel +420-5-4513-3350  
Fax +420-5-4521-2044  
Email heger@mendelu.cz

inhibit phosphorylation-driven signal transduction by a sterical competition with ATP or other ligands at the catalytic binding site of tyrosine kinases.<sup>3,4</sup> Despite the great success of TKIs, their usage is impeded by various side effects including sub-ungual hemorrhages, periorbital edema, anemia, thrombo- or neutropenia, nausea or diarrhea.<sup>5</sup> Moreover, the therapeutic window of TKIs is drastically narrowed by their poor bioavailability, acquired chemoresistance due to their low-efficiency uptake and systemic toxicity caused by interactions between TKIs and healthy tissue.<sup>6–8</sup> In addition, TKIs willingly interact with plasma proteins.<sup>9</sup> These phenomena undesirably affect TKIs' biodistribution, metabolism and elimination processes.<sup>10</sup> Therefore, selective drug delivery systems (DDS) able to obliterate the drawbacks of TKIs-based anticancer therapy are of utmost interest. Up to this date, a plethora of DDS have been employed for loading and delivery of various types of TKIs (comprehensively reviewed in recent review by Smidova et al<sup>11</sup>). However, it must be noted that a large portion of DDS suffer from DDS-type specific drawbacks including lack of biodegradability, low stability, structural heterogeneity or cyto-/immunotoxicity. Such disadvantages could be overcome by utilizing protein-based DDS originating from target organism (such as albumin, transferrin or ferritin).<sup>12</sup>

Ferritins (FRTs), the major iron storage and detoxifying proteins in most organisms, belong to the most promising biomacromolecular DDS.<sup>13</sup> The main role of FRTs is to prevent the harmful redox reactions in the organism by collecting free iron in the form of ferrihydrite phosphate in its core for a further use in enzyme cofactors.<sup>14</sup> In nature, the interior of FRTs is filled with iron, but when they are expressed artificially under iron-free conditions, the yielded apoFRTs are hollow, comprising a cavity that can be loaded with distinct types of bioactive compounds.<sup>15–21</sup> The uniqueness of FRTs lies in the fact that the protein can be reversibly dissociated into 24 (*H*- and/or *L*-) subunits through changes of pH from approx. 4 to 7.4 to enable encapsulation of the chosen cargo into its cavity.<sup>22</sup> This process could offer highly reproducible production of bio-compatible homogeneous DDS with plenty of choices for surface or structural modifications. On the other hand, harsh conditions of the low pH environment can have undesirable effects on a payload functionality. For instance, Khattab and coworkers have shown that incubation of AG-1478 (EGFR-targeted TKI) in acidic pH results in a formation of two twisted conformers, protonated at different quinazolyl nitrogen moiety.<sup>23</sup> Similar findings were also achieved with Gefitinib (EGFR-targeted TKI).<sup>24</sup> To avoid such prototropic

and geometric alterations, payload can be passively soaked through channels at the junctions of FRT subunits without disassembling the FRTs' structure.<sup>25,26</sup>

Another important feature of FRTs as DDS is that targeting ligands can be introduced to the FRTs' surface through a plethora of chemical or genetic modifications. Importantly, even non-modified FRTs can intrinsically target cancer cells through interaction with target receptors (TfR1 for *L*-rich FRTs or SCARA5 for *H*-rich FRTs), which are frequently up-regulated in several types of cancers.<sup>27</sup>

We herein report that horse (*Equus caballus*) spleen *L*-subunit-rich (22/2) FRTs can serve as efficient DDS for lenvatinib (Len, Lenvima<sup>®</sup>) and vandetanib (Van, Caprelsa<sup>®</sup>). Len and Van are multi-receptor TKIs that bind in the ATP-binding pocket of the active receptor kinase conformation and are well-known for their efficiency accompanied by a variety of undesired side events.<sup>28</sup> Considering the structural susceptibility of TKIs to acidic pH, we conducted a comparative evaluation on the effects of passive TKI diffusion versus their acidic pH-dependent encapsulation on a distinct physico-chemical and biological parameters. To the best of our knowledge, this has not previously been reported. In addition, to improve the active tumor cell-targeting properties of TKIs-loaded FRTs, we demonstrate a suitability of folate targeting as Trojan horse process utilizing folic acid (FA) as a surface immobilized ligand to target folate receptors (FR) frequently overexpressed on a variety of cancer cells with only a restricted expression in normal tissues.<sup>29,30</sup> Taken together, the presented study demonstrates that TKIs can be simply soaked into the FRTs to form actively targeted DDS without the need of utilizing the harsh encapsulation conditions.

## Materials and Methods

### Chemicals

Chemicals were purchased from Merck KGaA (Darmstadt, Germany) in ACS purity, unless noted otherwise. Milli-Q<sup>®</sup> (prepared using Barnstead GenPure UV Water Purification system, Thermo Fisher Scientific, Waltham, MA, USA) water was used throughout.

### Active and Passive Loading of TKIs into FRT DDS and Surface Functionalization with FA

TKIs nanoformulations were prepared via two different methods. The first was based on active encapsulation of TKIs (LC Laboratories, Woburn, MA, USA) into FRTs

utilizing an intrinsic property of FRTs to be reversibly disassembled due to pH changes. The solution consisting of 100  $\mu$ L of water, 200  $\mu$ L of Van or Len (1 mg/mL) in dimethylsulfoxide (DMSO) and 20  $\mu$ L of FRT (50 mg/mL) was mixed and incubated at 25°C. This step was followed by an addition of 0.75  $\mu$ L of 1 M HCl to maintain pH  $\sim$ 4.0, and stirring (15 min, 25°C), during which disassembly of the FRTs quaternary structure into subunits and incorporation of TKI occurred. The FRT reassembly was performed by adding 300  $\mu$ L of phosphate buffer (150 mM, pH 7.5) followed by incubation at 25°C, 15 min. The nanoformulations were then purified from the unencapsulated TKIs by diafiltration through Amicon®Ultra (50 K) columns (Sigma-Aldrich, St. Louis, MO, USA) (6000 $\times$  rcf, 20°C, 15 min, 3 $\times$ ) and refilled to the initial volume.

Passive diffusion was based on a spontaneous soaking of the hydrophobic TKIs through the channels at the junctions of FRTs subunit triplets. For this purpose, 100  $\mu$ L of water, 200  $\mu$ L of Van or Len (1 mg/mL) in DMSO and 20  $\mu$ L of FRT (50 mg/mL) was mixed and incubated at 25°C, 24 h. Then, the nanoformulations were purified from the unencapsulated TKIs by diafiltration through Amicon®Ultra (50 K) columns (6000 $\times$  rcf, 20°C, 15 min, 3 $\times$ ) and refilled to the initial volume.

The surface functionalization was achieved by incubation (600 $\times$  rpm, 25°C, 2 h) of 250  $\mu$ L of TKIs loaded in FRTs with 17.5  $\mu$ L of FA (56 mM in 1 M NaOH) and

25  $\mu$ L of *N,N'*-dicyclohexylcarbodiimide (DCC, 200 mM in DMSO). After incubation, the free FA was removed by diafiltration through Amicon®Ultra (50 K) columns (6000 $\times$  rcf, 20°C, 15 min, 3 $\times$ ). After the last centrifugation, FRTs were refilled to the original volume and stored for further use. Loading protocols together with structural formulas of payloads (Van and Len) and expected modes of binding of FA to the surface of TKIs-loaded FRT through DCC are schematized in Figure 1.

## Evaluation of Encapsulation and Surface Functionalization Efficiencies

The encapsulation efficiency (EE%) calculation was based on the absorption maxima of Van and Len ( $\lambda$ =320 nm). For quantitation, absorption spectra of TKIs were recorded prior and post diafiltration. EE% was calculated using Eq. (1):

$$EE\% = \frac{[\text{TKI added}] - [\text{free "unencapsulated TKI"}]}{[\text{TKI added}]} \times 100 \quad (1)$$

Similarly, FA surface binding was calculated through its absorption maximum ( $\lambda$ =365 nm). For this purpose, absorption spectra of FA immobilized on surface-modified TKIs-loaded FRTs were recorded prior and post diafiltration and the amount of immobilized FA was calculated from FA absorbance-based calibration curve. All efficiency analyses were conducted using spectrofluorimeter Tecan Infinite 200 PRO (Tecan, Mannedorf, Switzerland).

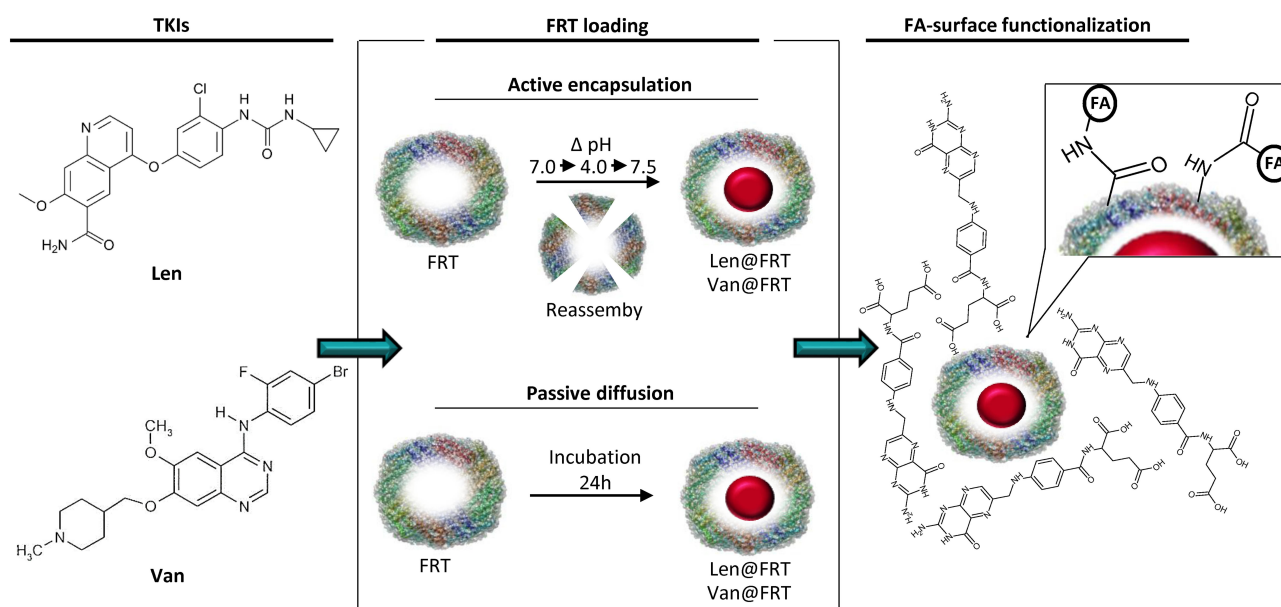


**Figure 1** Structural formulas of Len and Van employed as payloads for L-subunit-rich FRT DDS and schematic depiction of two TKIs-loading approaches and FA-surface functionalization. Note the two possible binding modes of FA to the surface of FRT enabled through zero-length linker DCC (detailed FRT surface zoomed in the rectangle). **Abbreviations:** Len, lenvatinib; Van, vandetanib; FRT, ferritin; DDS, drug delivery system; TKIs, tyrosine kinase inhibitors; FA, folic acid; DCC, *N,N'*-dicyclohexylcarbodiimide.

## Validation of FRTs Reassembly After TKIs Loading

Upon encapsulation and surface functionalization, proper reassembly was validated. This was particularly crucial for active encapsulation based on reversible dissociation of FRTs quaternary structure. Reassembly validation was performed using native polyacrylamide gel electrophoresis (N-PAGE). Briefly, 10  $\mu$ L of TKIs nanoformulations was mixed with 5  $\mu$ L of native loading buffer. Separation was carried out in native running buffer for 20 min at 200 V and 4°C. The gels were stained with Coomassie brilliant blue (CBB) and visualized using Azure c600 (Azure Biosystems, Dublin, CA, USA). In addition, TKIs-loaded FRTs were investigated using atomic force microscopy (AFM). Hybrid mode imaging (PeakForce QNM, PFQNM) was performed by the use of Bruker Dimension Icon AFM microscope (Bruker NanoSurfaces, Santa Barbara, CA, USA) equipped with a silicon nitride probe Bruker SCANASYST-AIR (Bruker AFM Probes, Camarillo, CA, USA). The basic probe parameters were calibrated by analysis of the measured thermal noise – cantilever sensitivity was 42.5 nm/V, spring constant 0.25 N/m. The nominal tip radius was 5 nm. The final post-processing and editing of the images were done using the Gwyddion software v. 2.55.<sup>31</sup>

## Investigation of Hydrodynamic Diameter and Stability of TKIs-Loaded FRTs

Hydrodynamic diameter (HDD) and  $\zeta$ -potential of TKIs-loaded FRTs were evaluated by dynamic light scattering on Zetasizer Nano ZS (Malvern Instruments, Malvern, UK). Upon dilution in water (100 $\times$ ), samples were placed into polystyrene latex cells and analyzed at a detector angle of 173°,  $\lambda=633$  nm and temperature of 25°C. Surface  $\zeta$ -potential was analyzed upon dilution of samples in water (20 $\times$ ) in a folded capillary cell. The number of runs varied between 20 and 40 and equilibration time was 120 s. In all analyses, the refractive index of dispersive phase and dispersive environment was set to 1.450 and 1.333, respectively.

## Evaluation of Release Kinetics of TKIs from TKIs-Loaded FRTs

Release kinetics of TKIs from TKIs-loaded FRTs was examined during incubation of TKIs-loaded FRTs in Ringer's solutions (RS, pH 7.4) or buffer mimicking acidic (hypoxic/endosomal) environment (0.142 g disodium phosphate, 6.650 g sodium chloride, 0.071 g sodium sulfate,

0.029 g calcium chloride dihydrate, 0.45 g glycine and 4.1 g potassium hydrogen phthalate in 1 L of water, pH 5.0) by capillary electrophoresis (Agilent 7100, Waldbronn, Germany) with UV/Vis detector. For separation, BGE buffer [(30 mM borate buffer, (20 mM) SDS, 5% EtOH)] was used. Separation conditions were as follows: voltage 25 kV, sample was injected hydrodynamically by 50 mBar pressure applied for 2 s. Between analyses, capillary was washed for 120 s by BGE. Between individual analyses, the samples were stored at 37°C.

## Evaluation of Protein Corona Formation

To investigate the hard protein corona formation, human plasma was mixed with TKIs-loaded FRTs at a 1:1 volume ratio to mimic the protein concentration in vivo (approx. 50% plasma in blood) and incubated for 35 min at 37°C and 350 rpm. After incubation, centrifugation (5 $\times$ , 30 min, 4°C, 21,130 $\times$  rcf) was conducted to remove unbound plasma proteins and pellet was resuspended and mixed with 5  $\mu$ L of non-reducing loading buffer. Samples were separated on sodium dodecyl sulfate polyacrylamide gel electrophoresis (SDS-PAGE) for 30 min at 200 V. The gels were stained via rapid CBB technique displayed using Azure c600 (Azure Biosystems).

## Hemocompatibility

Red blood cells (RBCs; Zen-Bio, Durham, NC, USA) were thawed and washed with 150 mM NaCl five-times. TKIs-loaded FRTs were diluted in phosphate-buffered saline (PBS, pH 7.4) to obtain 25.00, 15.50, 6.25 and 3.12  $\mu$ M TKIs. Each solution was mixed with RBCs at a 1:1 ratio and incubated (1 h, 37°C). Quantitation of hemolysis was performed according to the previously published protocol.<sup>15</sup>

## Cell Lines

For the purpose of the study, three human cell lines were utilized: i) the HBL-100, non-malignant cell line established from human milk, ii) T-47D and iii) MCF-7 representing estrogen-sensitive cell lines derived from a pleural effusion of ductal breast cancer. T-47D and MCF-7 cells were cultured in RPMI-1640, HBL-100 were cultured in DMEM. The culture media were supplemented with 10% fetal bovine serum (FBS), penicillin (100 U/mL) and streptomycin (0.1 mg/mL). Prior to each analysis, the cells were counted using automated cell counter Countess II FL (Thermo Fisher Scientific). All cell lines used in this study were purchased from American Type Culture Collection (Manassas, VA, USA).



## Evaluation of Antiproliferative Effects of TKIs-Loaded FRTs

Suspension of cells was seeded in 96-well plates (5000 cells per well) and incubated for 24 h. After that, the cells were treated with TKIs-loaded FRTs (normalized to 4  $\mu$ M concentration of TKIs) and incubated for 24 h. To quantify proliferation, the cells were stained using CyQUANT<sup>®</sup> GR kit (Thermo Fisher Scientific) according to the manufacturer's instructions. After staining, the fluorescence ( $\lambda_{\text{ex}}$  = 480 nm,  $\lambda_{\text{em}}$  = 520 nm) of samples was analyzed using Infinite 200 PRO (Tecan).

## Quantitation of Apoptosis

Cells were seeded in 6-well plates (600,000 cells per well) and incubated for 24 h. After treatment with TKIs-loaded FRTs and free TKIs (normalized to TKIs concentration of 4  $\mu$ M, 6 h) cells were detached using Accutase<sup>®</sup> (Sigma-Aldrich) followed by washing of cells suspension with cold PBS (2 $\times$ , 200 $\times$  ref, 10 min). For labeling, PE Annexin V Apoptosis Detection Kit I (BD Biosciences, San Jose, CA, USA) was utilized according to the manufacturer's instructions. Analyses were conducted using the BD Accuri C6 Plus (BD Biosciences) at 35  $\mu$ L/min through PE Annexin V (488 nm laser, 585/40 band-pass filter) and 7-AAD (488 nm laser, 670 long-pass filter) fluorescence. A minimum of 40,000 cells was analyzed per each group.

## Real-Time Quartz Crystal Microbalance (QCM)

TKIs-loaded and TKIs-free FRTs were immobilized on the surface of piezoelectric crystal covered with a gold layer. The 10 MHz Au/Ti coated QCM chips were purchased from International Crystal Manufacturing Company (Oklahoma City, OK, USA). The crystals were cleaned in acetone for 30 min and, afterwards, a monolayer of mercaptoundecanoic acid was formed (10 mg/mL in ethanol incubation for 1 h at 25°C). After washing of the surface with EtOH and water, the carboxylic groups were activated by 1 h incubation in the mixture of 200 mM 1-ethyl-3-(3-dimethylaminopropyl) carbodiimide and 50 mM *N*-hydroxysuccinimide in water. After washing with water, TKIs-loaded and TKIs-free FRTs were immobilized on the surface at the concentration of 0.4 mg/mL and the incubation was carried out overnight in wet atmosphere in the refrigerator. Prior to analyses, the piezoelectric crystals were placed in a flow-through cell. The measurements were performed using the QCM Analyzer (KEVA, Brno,

Czech Republic). The flow of the cell suspension was driven by the pump Minipul MP3 (Gilson, Villeurbanne, France). The whole system was controlled via the in-house developed software LabTools. The recorded parameters were resonant frequency  $f$ , autogain control voltage ( $R$ , corresponds to resistance of the crystal) and temperature in the cell; flow rate of cell suspension was 45  $\mu$ L/min.

## Confocal Laser Scanning Microscopy (CLSM)

TKIs-loaded FRTs were labelled with Cy3 NHS ester (Lumiprobe, Hannover, Germany). Cells were seeded to chamber slide (30,000 cells per well) and incubated overnight. Then, the cells were treated with Cy3 NHS ester-labelled TKIs-loaded FRTs (normalized to 4  $\mu$ M concentration of TKIs). After washing with PBS, cells were fixed using 200  $\mu$ L of 4% formaldehyde in PBS and incubated for 10 min at 25°C. The permeabilization of membranes was achieved by 100  $\mu$ L of 0.1% Triton X-100 in PBS. After blocking with 100  $\mu$ L of 3% BSA in PBS, the chamber slides were incubated with anti-Rab5 (PA3-915, dilution 1:250; Thermo Fisher Scientific), anti-FR (ab3361, dilution 1:100; Abcam, Cambridge, UK) or anti-LAMP1 (14-1079-80, dilution 1:100; Thermo Fisher Scientific) primary antibodies and incubated overnight at 4°C. After washing, the relevant FITC-labelled secondary antibodies were added and the slides were incubated at 4°C, 1 h. After washing with PBS-T (3 $\times$ ), each well was stained with Hoechst 33342. Stained slides were visualized using CLSM (LSM 880, Carl Zeiss, Jena, Germany)

## Clonogenic Assay

Cells were seeded into 6-well plates (1000 cells per well) and incubated for 24 h. Then, the cells were treated with TKIs-loaded FRTs and free TKIs (normalized to TKIs concentration of 8  $\mu$ M). After 6 h incubation, the treatment solutions were removed, the cells were washed gently with PBS, supplemented with fresh media and incubated until first visible colonies were formed. The cells were fixed using 3:1 methanol:acetic acid for 5 min and stained using 0.5% crystal violet in methanol for 15 min. Finally, the clonal efficiency was counted as the number of colonies containing at least 50 cells.

## Wound-Healing Assay

Cells were seeded into 6-well plates (100,000 cells per well) and incubated until 100% confluence was reached. To create

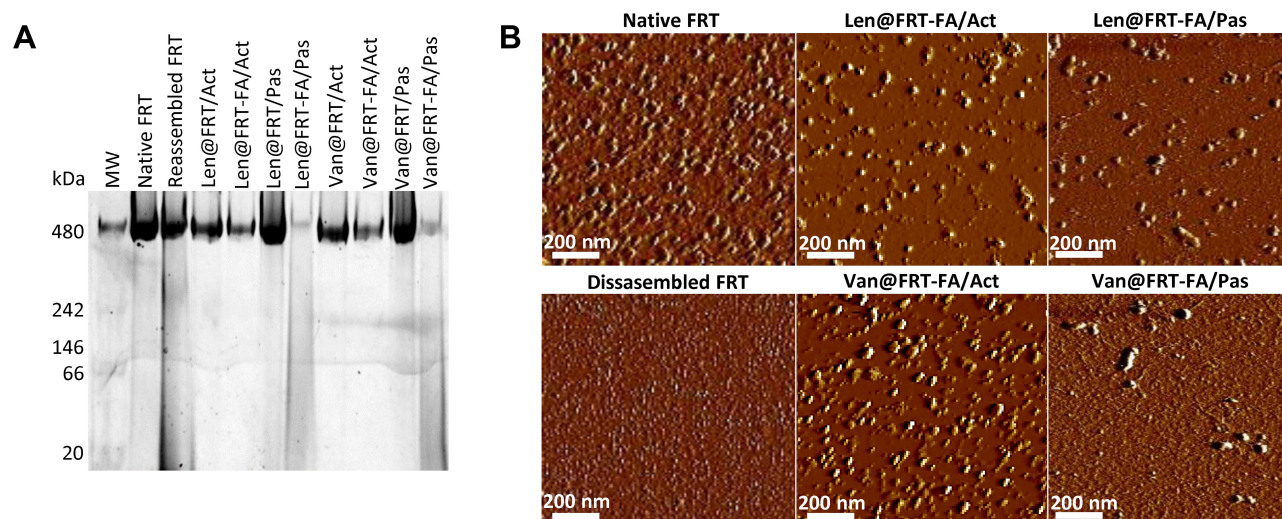


**Figure 2** Physico-chemical characterization of TKIs-loaded FRTs. **(A)** N-PAGE showing correct protein patterns for all prepared TKIs nanoformulations. After surface functionalization with FA, amount of FRT on the gel decreased due to some protein losses that occurred during a purification of unbound FA. **(B)** AFM micrographs of native and disassembled FRT and FA-modified TKIs-loaded FRTs. The values are expressed as a mean of three ( $n = 3$ ) independent replicates  $\pm$  SD.

**Abbreviations:** TKIs, tyrosine kinase inhibitors; FRT, ferritin; N-PAGE, native polyacrylamide gel electrophoresis; FA, folic acid; MW, weight marker; AFM, atomic force microscopy.

a cell-free zone, a line was scraped in each well with a p20 pipet tip, followed by washing with PBS. Then, the cells were treated with TKIs-loaded FRTs and free TKIs (normalized to TKIs concentration of 8  $\mu$ M). After 6 h incubation, the cells were supplemented with fresh media. Micrographs of artificial wound were captured using EVOS FL Auto Cell Imaging System (Thermo Fisher Scientific) for up to 12 days. The growth media were changed every 2 days.

## Descriptive Statistics

For the statistical evaluation of the results, the mean was taken as the measurement of the main tendency, while positive and negative error was taken as the dispersion measurement. Differences between groups were analyzed using unpaired *t*-test and ANOVA. For analyses, software Statistica 12 (StatSoft, Tulsa, OK, USA) was employed.

## Results and Discussion

### Physico-Chemical Characterization of TKIs-Loaded FRTs

For the purpose of TKIs-loading, commercially purified *E. caballus* spleen L-subunit-rich FRTs were utilized, with excelling biocompatibility, biodegradability, non-toxicity and high loading efficiency as has been previously demonstrated for a variety of bioactive compounds.<sup>15,17,20,21,32–34</sup> N-PAGE revealed that the FRTs were single protein complex with an apparent MW of about 480 kDa (**Figure 2A**). Upon pH-dependent reassembly w/o payload, FRTs

successfully retained their structural integrity and charge, which is in line with Stuhn et al.<sup>35</sup> Similar findings were further obtained for both types of TKIs loading. It must be noted that in comparison to passive diffusion, FRTs that underwent the active loading of TKIs exhibited some extent of concentration decline. This was most likely due to imperfect reassembly leading to a partial loss of protein subunits during diafiltration. In addition, losses of FRTs also occurred during FA-surface functionalization steps. Despite the fact that the amount of recovered FA-functionalized TKIs-loaded FRTs were still high enough, this phenomenon must always be taken into account and thoroughly checked.

DLS results confirmed that the native FRT and TKIs-loaded FRTs were relatively monodispersed with only a minor effect of FA-surface functionalization on FRTs HDDs (**Table 1**). Noteworthy, a passive diffusion of Van into FRTs resulted in elevation of HDD to approx. 30 nm. This might be attributed to increased affinity of Van to the FRT exterior causing a small portion of FRTs agglomeration. In water, native FRT exhibited  $\zeta$ -potential of  $-24.6$  mV. Passive diffusion of TKIs led to only negligible  $\zeta$ -potential changes ( $-26.1$  mV for Len and  $-27.0$  mV for Van, respectively) indicating only a minor alteration of FRTs' surface properties. In contrast, FRTs subjected to active pH-dependent encapsulation exhibited a marked decrease in  $\zeta$ -potentials ( $-6.5$  mV for Len and  $-14.5$  mV for Van, respectively). This suggests that even though FRTs were thoroughly purified after the

**Table 1** Physico-Chemical Parameters of TKIs-Loaded FRTs

Sample	HDD (nm)	ζ-Potential (mV)	PDI	EE %	Drug Loaded (μM)	FA Immobilization Efficiency (%)	FA Immobilized (μM)
Native FRT	11.7	−24.60	~0.316	–	–	–	–
Len@FRT/Act	11.9	−6.53	~0.468	25.3	184.9	–	–
Len@FRT-FA/Act	13.5	−16.41	~0.282	–	–	2.06	69.7
Len@FRT/Pas	12.0	−26.17	~0.532	20.7	203.4	–	–
Len@FRT-FA/Pas	11.8	−30.11	~0.343	–	–	1.94	60.1
Van@FRT/Act	17.5	−14.53	~0.468	8.4	55.4	–	–
Van@FRT-FA/Act	12.0	−16.55	~0.356	–	–	2.00	69.1
Van@FRT/Pas	17.7	−29.14	~0.385	14.5	143.4	–	–
Van@FRT-FA/Pas	27.8	−27.05	~0.256	–	–	1.76	55.4

**Abbreviations:** FRT, ferritin; HDD, hydrodynamic diameter; PDI, polydispersity index; EE%, encapsulation efficiency; FA, folic acid.

pH-dependent encapsulation of TKIs, they most likely retained some portion of the acidic environment in their structure affecting their ζ-potential values.<sup>36</sup> Therefore, it can be speculated that in contrast to passive diffusion, active loading of TKIs into surface-unmodified FRTs can have deleterious effects on their stability. In all samples, surface functionalization with FA resulted in a slight decrease in ζ-potentials.

It is worth noting that Van and Len are hydrophobic drugs with lateral dimensions (~0.3 nm) allowing passive diffusion through 4-fold hydrophobic channels in the FRT structure (~0.5 nm).<sup>37,38</sup> Therefore, in terms of EE% of Len, only small differences were found between active vs passive loading. In contrast, Van was found to be more efficiently loaded into FRTs by passive diffusion (Table 1). These data highlight that hydrophobic molecules, which form a substantial part of chemotherapeutics, can be simply loaded into FRT-based DDS by passive diffusion without the need of reassembly process utilizing the harsh acids-based conditions.

Folate targeting is a highly efficient active delivery approach that has been exploited for a broad spectrum of nanomedicines (reviewed in Bazak et al<sup>39</sup>). Hence, we employed this principle and surface-functionalized TKIs-loaded FRTs to bestow active-targeting capabilities towards cells with high level of FR expression. For this purpose, we utilized a DCC-mediated chemical coupling of FA,<sup>40</sup> which resulted in a successful immobilization of FA on the surface of TKIs-loaded FRTs. It should be noted that all passively-loaded FRTs exhibited slightly lower FA functionalization efficiency suggesting that some of the passively loaded TKIs could be partially bound to the surface of FRTs and occupy the binding sites for DCC coupling.

AFM micrographs in Figure 2B show a typical size and homogeneous distribution of native FRTs. Upon pH-dependent disassembly, laterally small objects, most likely

protein subunits, were found confirming the sufficiency of utilized acidic conditions (pH 4.0) for FRT disassembly. Noteworthy, compared to the actively-loaded FRTs, AFM revealed that passive loading of FRTs with Van resulted in a formation of some amount of agglomerates, which is in line with the DLS analysis. Nonetheless, the resulting size (~30 nm) complies with the generally accepted requirements for a size of nanoparticles for medical applications.<sup>41</sup> It was further found that compared to active encapsulation, passively loaded FRTs exhibited a lower focal adhesion, which is plausibly due to their considerably lower surface ζ-potential affecting their non-covalent interactions with AFM tip (Figure S1). In addition, nano-mechanical analyses of FRTs' deformation revealed that in general, actively-loaded TKIs exhibited a higher force sensitivity. This phenomenon can be attributed to structural defects due to improper folding of FRTs that can occur during the pH-dependent reassembly.<sup>42</sup> Rigidity of TKIs-loaded FRTs was further increased after surface functionalization, validating the presence of FA on the surface of TKIs-loaded FRTs.

## In vitro Prediction of Biocompatibility of TKIs-Loaded FRTs

In order to predict the biocompatibility of TKIs-loaded FRTs, we first determined their stability in RS, which is an isotonic solution mimicking the environment of mammalian extracellular fluids<sup>43</sup> and acidic buffer mimicking hypoxic/endosomal environment. In case of Len, both loading processes exhibited a similar premature release of the payload. The highest release of Len was observed in the shorter incubation periods, whilst samples that were subjected to longer incubation periods (24 h) exhibited only minimal release of Len (Figure 3A). Interestingly,

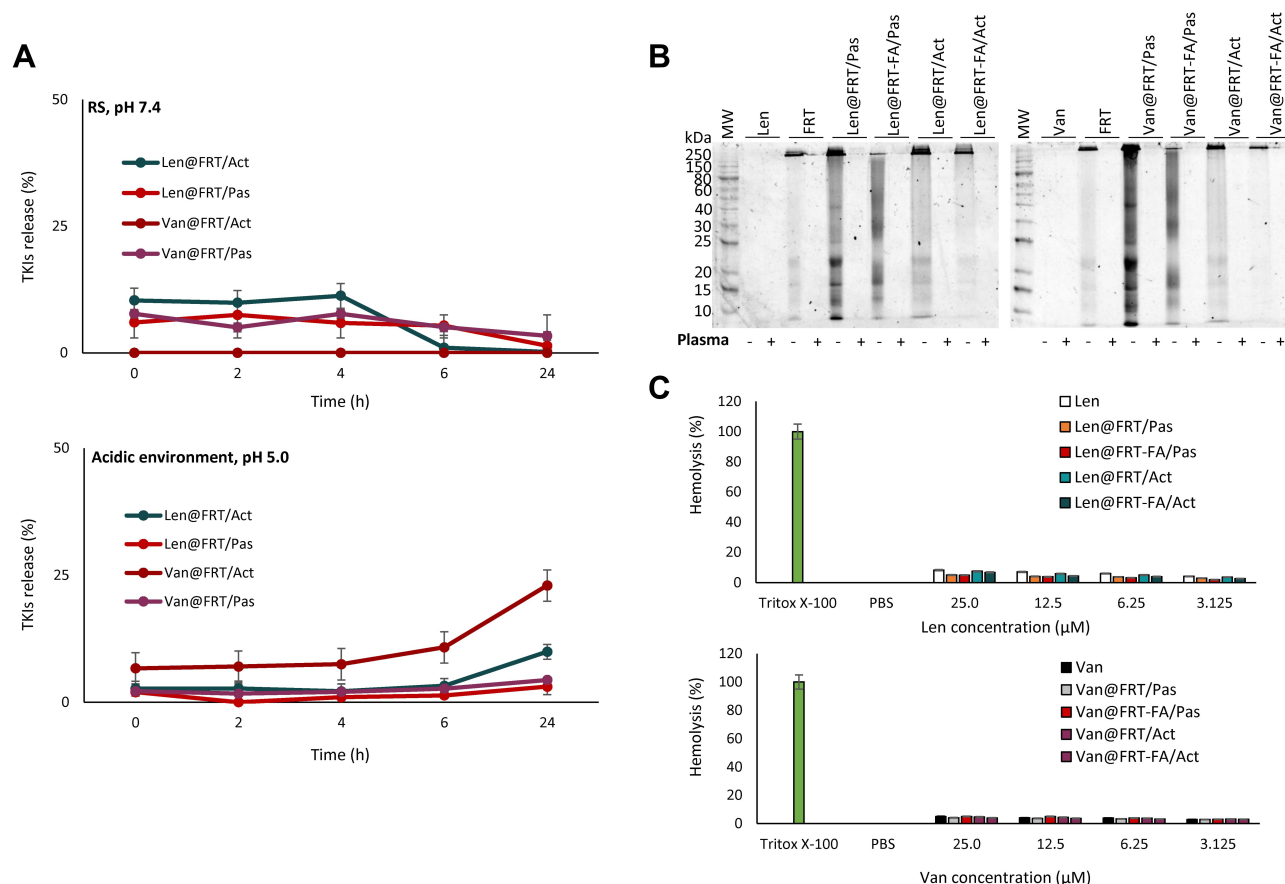


**Figure 3** Evaluation of in vitro biocompatibility of TKIs-loaded FRTs. **(A)** Release kinetics of Van and Len from TKIs-loaded FRTs during incubation in RS (pH 7.4) or acidic buffer (pH 5.0), respectively. The values are expressed as a mean of three ( $n = 3$ ) independent replicates  $\pm$  SD. **(B)** Hard human plasma protein corona profiles eluted on SDS-PAGE (denoted with +). Denoted with – are SDS-PAGE profiles of individual TKIs or their nanoformulations. **(C)** Ex vivo examination of possible hemolysis of TKIs-loaded FRTs assayed on human RBCs. PBS (pH 7.4) and Triton X-100 are shown as negative and positive controls, respectively.

**Abbreviations:** TKIs, tyrosine kinase inhibitors; FRT, ferritin; SD, standard deviation; SDS-PAGE, sodium dodecyl sulfate polyacrylamide gel electrophoresis; RBCs, red blood cells; PBS, phosphate-buffered saline.

while passively-loaded Van exhibited similar release curve as Len nanoformulations, active loading of Van resulted in a highly stable DDS in which virtually no premature release was found in all aliquots incubated in RS. Although we cannot provide experimental data to explain this phenomenon, high repeatability of this analysis underpins that in RS, actively-loaded Van is tightly bound to the FRT. These data suggest that RS can have capability to stabilize the payload in the FRTs. Hence, it can be anticipated that the 24 h pre-incubation of TKIs-loaded FRTs in RS can be a stabilizing step preceding future in vivo applications. It must be noted that acidic pH of hypoxic microenvironment (pH  $\sim$ 6.5) of solid tumors and endolysosomal compartments (pH  $>$   $\sim$ 5.0) can have a dramatic effect on release of TKIs. Therefore, we further investigated release kinetics of TKIs during incubation in acidic, hypoxia/endosomal compartments-mimicking buffer (pH 5.0). It was found the acidic pH triggers lower burst

release (0 h) of TKIs compared to RS (Figure 3A). Moreover, in contrast to RS, incubation in acidic buffer led to a slow sustained release of TKIs observed particularly for actively-loaded FRTs but not for their passively-loaded counterparts suggesting a decreased stability of FRTs structure due to the active pH-dependent encapsulation protocol, which is in line with our physico-chemical characterization data.

Biocompatibility with blood environment is a crucial parameter for any therapeutical modality intended for intravenous (*i.v.*) administration. Exceptional hemocompatibility of FRT has been studied in our previously published study.<sup>20</sup> However, the loading protocol, type of payload and surface functionalization can affect hemocompatibility of DDS.<sup>44</sup> Thus, we first analyzed whether TKIs-loaded FRTs adsorb a protein corona from human plasma. Noteworthy, practically no formation of hard plasma protein corona was found irrespective of FA



surface functionalization (Figure 3B). This is of particular importance since protein corona can effectively shield the targeting ligands or recognition units on the DDS surface, thus affecting biodistribution and specificity of delivery process.<sup>45</sup> In addition, all formulations of TKIs-loaded FRTs exhibited a neglectable or no destruction of human RBCs and consequent release of hemoglobin (Figure 3C and Figure S2). Taken together, the results suggest a great biocompatibility of TKIs-loaded FRTs with a bloodstream environment and underpin their suitability for *i.v.* administration.

## Cytotoxicity of TKIs-Loaded FRTs and Selectivity of FA Surface Functionalization

Although Len and Van have been approved and are primarily used for chemotherapeutic interventions in advanced radioiodine refractory/medullary thyroid cancers and unresectable hepatocellular carcinoma,<sup>46,47</sup> they have also been recently

registered to the clinical trials for single agent or combination therapy for hormone-responsive breast cancer (ClinicalTrials.gov Identifiers: NCT03168074, NCT02562118 and NCT002530411). Therefore, to examine the efficiency of TKIs-loaded FRTs, we utilized two cell lines derived from hormone (progesterone/estrogen)-responsive breast cancers (T-47D and MCF-7). Both cell lines are VEGFR-positive,<sup>46</sup> predetermining them as suitable targets for TKIs-based therapy. In addition,<sup>30,48</sup> both cell lines exhibit high expression of FR [ $>28$ -fold (T47-D) and  $>11$ -fold (MCF-7) higher compared to healthy HBL-100 cells] and comparable expression of TfR1 (a receptor with affinity to L-rich FRTs) (Figure S3). Therefore, they are ideal *in vitro* models for evaluation of FA-mediated targeting of TKIs-loaded FRTs.

We first focused on antiproliferative effects of TKIs-loaded FRTs with a special emphasis on functionality of folate targeting. Figure 4A demonstrates that in control HBL-100 cells, TKIs-loading had only minimal effect on proliferation. Since HBL-100 cells express only

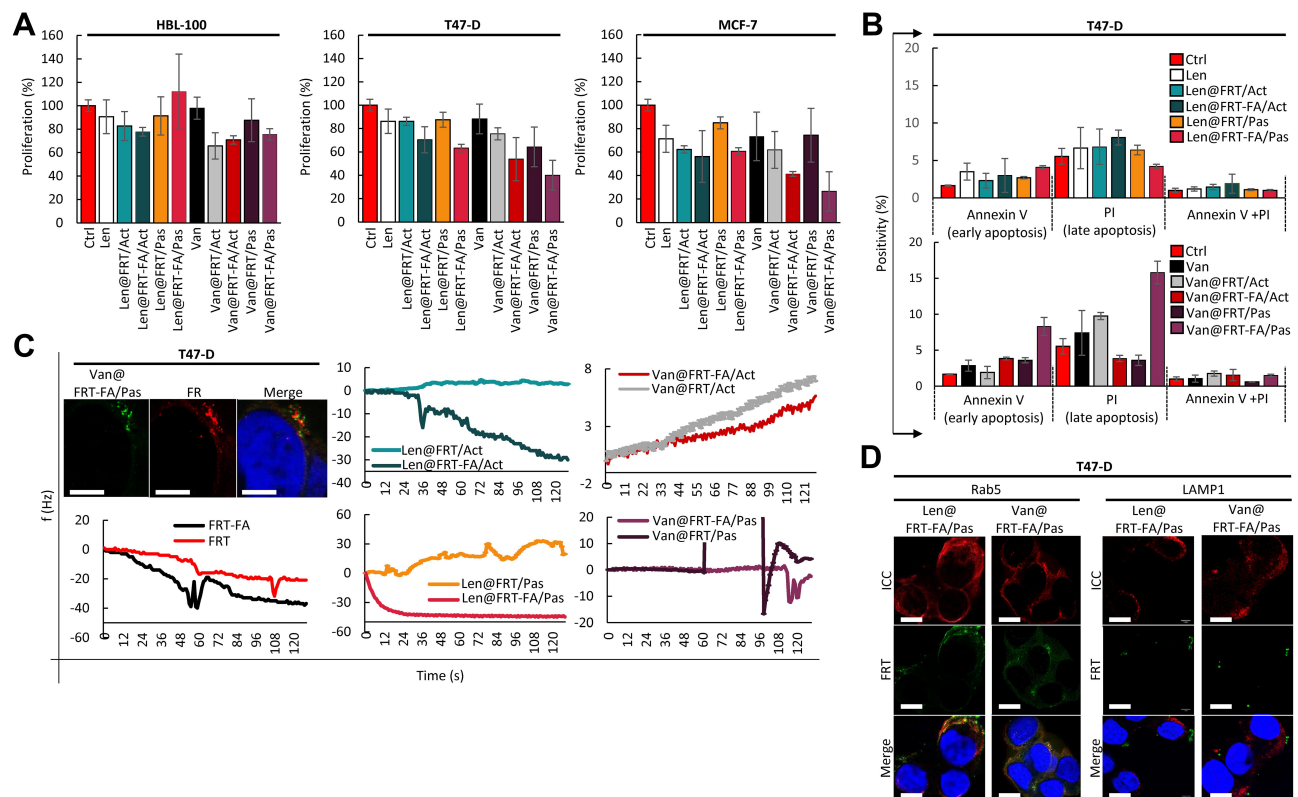


**Figure 4** Evaluation of cytotoxicity, selectivity and intracellular fate of TKIs-loaded FRTs. (A) Antiproliferative effects of TKIs-loaded FRTs. (B) Capability of TKIs-loaded FRTs to induce apoptosis in target T47-D cells. (C) QCM analysis of efficiency of FA targeting compared to surface-unmodified TKIs-loaded FRTs. QCM was performed in FR overexpressing T47-D cells. Representative CLSM micrographs shown in inset demonstrate a co-localization of Cy3-labeled Van@FRT-FA/Pas with FR upon 5 min treatment of T47-D cells. Scale bar, 5  $\mu$ m. (D) CLSM micrographs showing a fast association (after 5 min exposure) of Cy3-labeled FA-targeted TKIs-loaded FRTs with endosomal compartment and only negligible co-localization of TKIs-loaded FRTs with lysosomes post 24 h exposure. Scale bar, 10  $\mu$ m. The values are expressed as the mean of three ( $n = 3$ ) independent replicates  $\pm$  SD.

**Abbreviations:** TKIs, tyrosine kinase inhibitors; FRT, ferritin; QCM, quartz crystal microbalance; FA, folic acid; FR, folate receptor; CLSM, confocal laser scanning microscopy; Van, vandetanib; Len, lenvatinib; SD, standard deviation.

a negligible amount of FR,<sup>17</sup> slight increase in cytotoxicity of Van and Len loaded in FRT can be attributed to some extent to the interactions between TfR1 expressed on surface of HBL-100 cells and FRTs,<sup>49</sup> enabling a facile intracellular accumulation of TKIs triggering consequent multiple kinase inhibitory activity. This is in line with the results showing that FA-surface functionalization plausibly acting as a sterical hindrance on the FRTs domains with affinity to TfR1, mostly resulted in a decrease in TKIs cytotoxicity in HBL-100 cells. In contrast, in FR expressing T47-D and MCF-7 cells, FA functionalization substantially stimulated antiproliferative effects of TKIs-loaded FRTs, while in both cell lines, the highest antiproliferative activity was found for Van@FRT-FA/Pas. This is in agreement with a quantitation of induction of apoptosis examined in T-47D cells, in which Van@FRT-FA/Pas treatment led to the highest rate of early/late apoptotic cells (Figure 4B). For Len, only a slight induction of apoptosis was found throughout the short-term treatments, suggesting a slower onset of its inhibitory activity compared to Van. It is worth noting that the antiproliferative effects and induction of apoptosis have been evaluated in a 24 h experiment that was primarily focused on validation of functionality of folate targeting. Considering the mechanism of action of TKIs, there is no doubt that longer administration times will result in a more profound cytotoxic effect<sup>50</sup> that will enable the delineation of impact of loading pipeline on TKIs-loaded FRTs anticancer activity. The latter was investigated as well and will be discussed in the following chapter.

Due to the nature of the obtained data, next we put our attention on further validation of folate targeting. CLSM micrographs of Van@FRT-FA/Pas administration in T47-D cells (inset in Figure 4C) show numerous punctate spots corresponding to Cy3-labeled FRTs co-localized with the area of high expression of FR clustering on the cell surface. This phenomenon is generally followed by a ligand invagination to form an early endosome.<sup>51</sup> A fast and efficient folate targeting was further corroborated by QCM demonstrating a considerable lower frequency in FA-functionalized FRTs highlighting a fast and efficient binding of T47-D cells on the FRTs-coated surface of QCM chips. All in all, the gathered data validated the folate targeting as a suitable choice for actively-targeted nanomedicine of TKIs utilizing FRTs as DDS.

FA-drug/nanoparticles conjugates that bind to the FR trigger cellular uptake via receptor-mediated endocytosis.<sup>52</sup> Indeed, we observed a large portion of TKIs-loaded FRTs

co-localizing with Rab5, which localizes on early endosomes (Figure 4D). Importantly, multivalent FA conjugates traffic quickly from endosomes to lysosomes with the pH of compartments ~5.0, in which any digestible content is processed by lysosomal enzymes.<sup>53</sup> Considering the fact that several studies have shown that the release of a payload from FRTs is enabled by activity of lysosomal enzymes,<sup>54,55</sup> upon endocytosis, FRTs are digested in lysosomes, which most likely results in the release of Cy3 label from FRTs and its passing outside the lysosomes as evidenced by LAMP1 staining (Figure 4D). FRTs digestion enables small hydrophobic TKIs to diffuse through the lysosomal membrane into the intracellular space. This feature must be taken into account, since only TKIs that can exert inhibitory activity through binding to intracellular tyrosine kinase domain (Van, Len, sunitinib, sorafenib, etc.<sup>56</sup>) can thus serve as a payload for FRTs. Importantly, the intracellular fate investigations did not reveal any substantial differences between behavior of passive and active loading of TKIs, suggesting that both protocols are suitable for adaptation to drug delivery utilizing FRTs inherent receptor-mediated endocytic route.

## Long-Term Inhibitory Activity of TKIs-Loaded FRTs on Clonogenicity and Migration

To identify how the cells cope with the long-term challenge with TKIs-loaded FRTs, we first focused on the inhibitory activity of TKIs on clonal efficiency. The obtained data confirmed that in general TKIs require longer exposure times to fully exhibit their anticancer effects. Importantly, although we did not find marked differences between cytotoxicity of passively vs actively loaded FRTs in the short-term experiments, the long-term experiments revealed that passive loading of TKIs results in a considerably higher inhibitory effect. Figure 5A and B demonstrate that the treatment with passively loaded FRTs equipped with FR-targeting capabilities resulted in a marked decline of a number of progeny colonies. This phenomenon was particularly obvious in FR-positive T47-D and MCF-7 cells, while virtually no inhibition of clonal efficiency was found in healthy HBL-100 cells. Taken together with the fact that FA-unmodified TKIs-loaded FRTs exhibited only minimal differences in their inhibitory activities, most likely due to some extent of expression of TfR1/SCARA5, this finding underpins the utmost

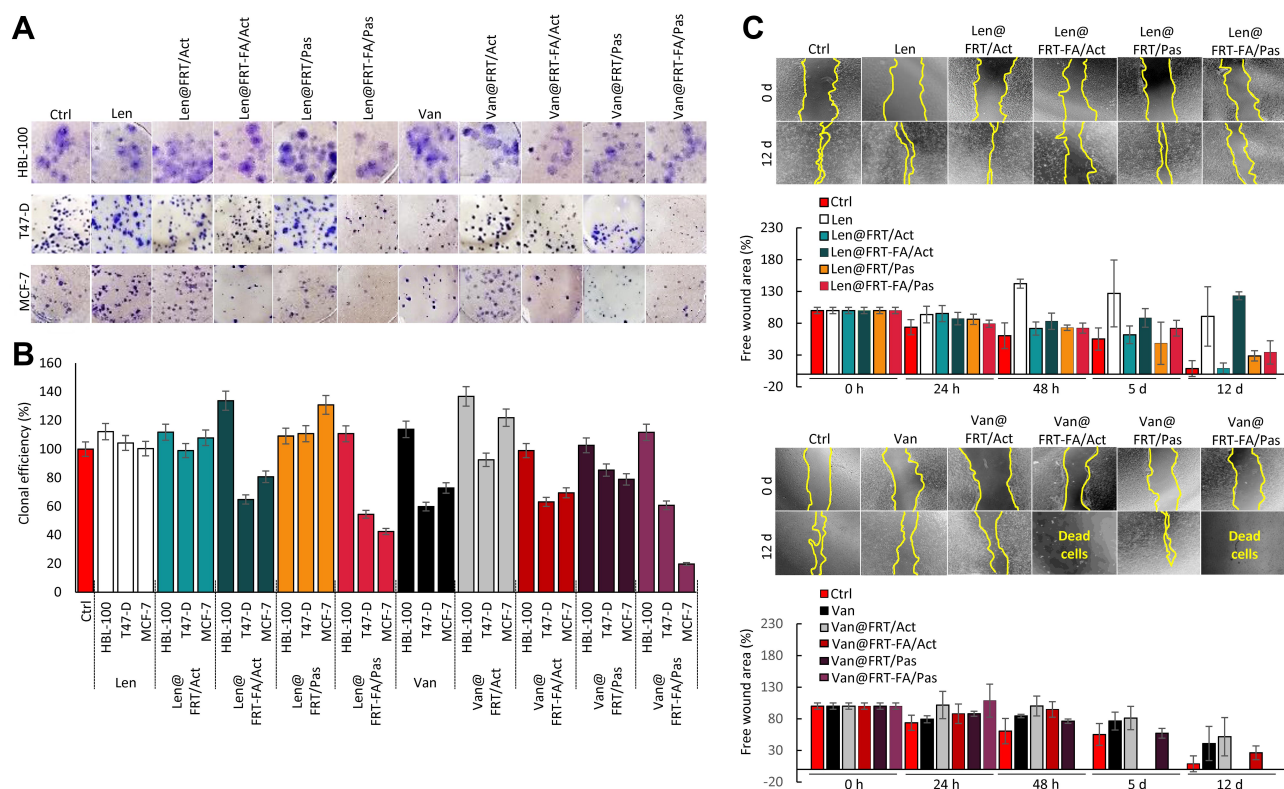


**Figure 5** FA surface functionalization of TKIs-loaded FRTs markedly accelerates inhibition of clonogenicity and migration in breast cancer cells. **(A)** Representative micrographs showing formation of colonies upon administration with annotated treatments. **(B)** Quantitation of clonal efficiency. **(C)** Representative micrographs showing the migration of T47-D cells upon administration with annotated treatments. Bar graphs depict percentage of free wound area. The values are expressed as the mean of three ( $n = 3$ ) independent replicates  $\pm$  SD.

**Abbreviations:** TKIs, tyrosine kinase inhibitors; FRT, ferritin; SD, standard deviation.

importance of folate targeting for a selective delivery of TKIs to breast cancer cells.

In line with the clonogenicity data, the evaluation of antimigratory activity of TKIs-loaded FRTs in T47-D cells confirmed slightly better performance of passively-loaded FRTs as well as the importance of folate targeting for stimulation of TKIs activity (Figure 5C). Noteworthy, upon administration with FA-functionalized actively and passively Van-loaded FRTs, no living cells were found after 48 h and 5 days, respectively, indicating their high cytotoxic performance in T47-D cells. Taken together, the long-term experiments revealed that passive loading is considerably beneficial over pH-dependent encapsulation of TKIs in terms of their resulting biological activity.

Last but not least, our results also demonstrate that Van is a better candidate for breast cancer therapy than Len. We attribute this phenomenon to the differences between kinase affinities of Van vs Len. Van exhibits its affinity not only to VEGFR, but also EGFR and RET-tyrosine kinase.<sup>57</sup> Previously published studies describing that expression of EGFR positively correlates with poor prognosis of

hormone-responsive breast cancers<sup>58</sup> and that expression of RET-tyrosine kinase is associated with estrogen receptor abundance<sup>59</sup> support our hypothesis. In contrast to Van, Len primarily targets VEGFR1/2/3,<sup>60</sup> whose expression is generally more frequent in HER2-positive or triple-negative breast cancer subpopulations.<sup>61,62</sup> Despite the involvement of representative cell lines might confirm this affirmation, such investigation was beyond the scope of this study.

## Conclusion

Successful loading of Van and Len through two distinct protocols into FRT-based DDS, facile surface functionalization with FA and subsequent differences in biological activity in the breast carcinoma cells are demonstrated. We show that despite both protocols being suitable for efficient loading of FRTs with Van and Len and neither of the loading protocols exhibiting an effect on the efficiency of surface functionalization with FA, the passive loading resulted in a more potent TKIs nanoformulations. This phenomenon is plausibly due to structural and functional changes in TKIs structure caused by exposure to acidic



pH. However, this statement requires further experimental validation. Our study demonstrates for the first time that FA-functionalized FRTs are highly promising and cancer cell-selective DDS for TKIs-based anticancer medicine. Importantly, since passive loading does not require a reassembly step for which acids are needed and which frequently results in improper folding of FRTs quaternary structure that can affect their further functional properties (stability, receptor affinity, payload release kinetics, etc.), the presented investigation will serve as a solid basis for all future studies focused on encapsulation of small hydrophobic molecules into FRTs. Overall, FRTs are safe and efficient DDS holding great potential for further clinical translation. Therefore, we envisage that particularly FA-functionalized passively loaded Van could be translated into in vivo settings and merits further investigation as a highly selective nano-based therapeutic modality for hormone-responsive breast cancers.

## Acknowledgments

We acknowledge CF Nanobiotechnology supported by MEYS CR (LM2018127).

## Funding

This work was supported by The Czech Science Foundation (project GACR 18-10251S), AF-IGA-IP-2019-IP073 and CEITEC 2020 (LQ1601).

## Disclosure

The authors report no conflicts of interest in this work.

## References

- Mann J. Natural products in cancer chemotherapy: past, present and future. *Nat Rev Cancer*. 2002;2(2):143–148. doi:10.1038/nrc723
- Sawyers C. Targeted cancer therapy. *Nature*. 2004;432(7015):294–297. doi:10.1038/nature03095
- Al-Obeidi FA, Lam KS. Development of inhibitors for protein tyrosine kinases. *Oncogene*. 2000;19(49):5690–5701. doi:10.1038/sj.onc.1203926
- Gross S, Rahal R, Stransky N, Lengauer C, Hoeflich KP. Targeting cancer with kinase inhibitors. *J Clin Invest*. 2015;125(5):1780–1789. doi:10.1172/JCI76094
- Caldemeyer L, Dugan M, Edwards J, Akard L. Long-term side effects of tyrosine kinase inhibitors in chronic myeloid leukemia. *Curr Hematol Malig Rep*. 2016;11(2):71–79. doi:10.1007/s11899-016-0309-2
- Herbrink M, Nuijen B, Schellens JHM, Beijnen JH. Variability in bioavailability of small molecular tyrosine kinase inhibitors. *Cancer Treat Rev*. 2015;41(5):412–422. doi:10.1016/j.ctrv.2015.03.005
- Zhang JM, Yang PL, Gray NS. Targeting cancer with small molecule kinase inhibitors. *Nat Rev Cancer*. 2009;9(1):28–39. doi:10.1038/nrc2559
- Haringhuizen A, van Tinteren H, Vaessen HFR, Baas P, van Zandwijk N. Gefitinib as a last treatment option for non-small-cell lung cancer: durable disease control in a subset of patients. *Ann Oncol*. 2004;15(5):786–792. doi:10.1093/annonc/mdh177
- Wani TA, Bakheit AH, Zargar S, Hamidaddin MA, Darwish IA. Spectrophotometric and molecular modelling studies on in vitro interaction of tyrosine kinase inhibitor linifanib with bovine serum albumin. *PLoS One*. 2017;12(4):1–12. doi:10.1371/journal.pone.0176015
- Hauouala A, Widmer N, Duchosal MA, Montemurro M, Buclin T, Decosterd LA. Drug interactions with the tyrosine kinase inhibitors imatinib, dasatinib, and nilotinib. *Blood*. 2011;117(8):75–87. doi:10.1182/blood-2010-07-294330
- Smidova V, Michalek P, Goliasova Z, et al. Nanomedicine of tyrosine kinase inhibitors. *Theranostics*. 2020.
- Tesarova B, Musilek K, Rex S, Heger Z. Taking advantage of cellular uptake of ferritin nanocages for targeted drug delivery. *J Control Release*. 2020;325:176–190. doi:10.1016/j.jconrel.2020.06.026
- Ebrahimi KH, Bill E, Hagedoorn PL, Hagen WR. The catalytic center of ferritin regulates iron storage via Fe(II)-Fe(III) displacement. *Nat Chem Biol*. 2012;8(11):941–948. doi:10.1038/nchembio.1071
- Tosha T, Hasan MR, Theil EC. The ferritin Fe<sub>2</sub> site at the diiron catalytic center controls the reaction with O<sub>2</sub> in the rapid mineralization pathway. *Proc Natl Acad Sci U S A*. 2008;105(47):18182–18187. doi:10.1073/pnas.0805083105
- Tesarova B, Dostalova S, Smidova V, et al. Surface-PASylation of ferritin to form stealth nanovehicles enhances in vivo therapeutic performance of encapsulated ellipticine. *Appl Mater Today*. 2020;18:1–10.
- Indra R, Cerna T, Heger Z, et al. Ellipticine-loaded apoferritin nanocarrier retains DNA adduct-based cytochrome P450-facilitated toxicity in neuroblastoma cells. *Toxicology*. 2019;419:40–54. doi:10.1016/j.tox.2019.03.009
- Tesarova B, Charousova M, Dostalova S, et al. Folic acid-mediated re-shuttling of ferritin receptor specificity towards a selective delivery of highly cytotoxic nickel(II) coordination compounds. *Int J Biol Macromol*. 2019;126:1099–1111. doi:10.1016/j.ijbiomac.2018.12.128
- Peskova M, Ilkovics L, Hynek D, et al. Detergent-modified catalytic and enzymomimetic activity of silver and palladium nanoparticles biotemplated by *Pyrococcus furiosus* ferritin. *J Colloid Interface Sci*. 2019;537:20–27. doi:10.1016/j.jcis.2018.11.005
- Pekarik V, Peskova M, Guran R, et al. Visualization of stable ferritin complexes with palladium, rhodium and iridium nanoparticles detected by their catalytic activity in native polyacrylamide gels. *Dalton Trans*. 2017;46(40):13690–13694. doi:10.1039/C7DT02818K
- Dostalova S, Cerna T, Hynek D, et al. Site-directed conjugation of antibodies to apoferritin nanocarrier for targeted drug delivery to prostate cancer cells. *ACS Appl Mater Interfaces*. 2016;8(23):14430–14441.
- Dostalova S, Polanska H, Svobodova M, et al. Prostate-specific membrane antigen-targeted site-directed antibody-conjugated apoferritin nanovehicle favorably influences in vivo side effects of doxorubicin. *Sci Rep*. 2018;8:1–13.
- Heger Z, Skalickova S, Zitka O, Adam V, Kizek R. Apoferritin applications in nanomedicine. *Nanomedicine*. 2014;9(14):2233–2245. doi:10.2217/nnm.14.119
- Khattab M, Wang F, Clayton AHA. A pH-induced conformational switch in a tyrosine kinase inhibitor identified by electronic spectroscopy and quantum chemical calculations. *Sci Rep*. 2017;7:1–10. doi:10.1038/s41598-017-16583-z
- Huang Y, Hu QH, Song GX, et al. Cucurbit 7,8 urils binding to gefitinib and the effect of complex formation on the solubility and dissolution rate of the drug. *RSC Adv*. 2014;4(7):3348–3354. doi:10.1039/C3RA45017A
- Liu XF, Jin WL, Theil EC. Opening protein pores with chaotropes enhances Fe reduction and chelation of Fe from the ferritin biomineral. *Proc Natl Acad Sci U S A*. 2003;100(7):3653–3658. doi:10.1073/pnas.0636928100
- Zhen ZP, Tang W, Guo CL, et al. Ferritin nanocages to encapsulate and deliver photosensitizers for efficient photodynamic therapy against cancer. *ACS Nano*. 2013;7(8):6988–6996. doi:10.1021/nn402199g



27. Zhang LB, Li L, Di Penta A, et al. H-chain ferritin: a natural nuclei targeting and bioactive delivery nanovector. *Adv Healthc Mater.* **2015**;4(9):1305–1310. doi:10.1002/adhm.201500226
28. Cabanillas ME, Habra MA. Lenvatinib: role in thyroid cancer and other solid tumors. *Cancer Treat Rev.* **2016**;42:47–55. doi:10.1016/j.ctrv.2015.11.003
29. Fernandez M, Javaid F, Chudasama V. Advances in targeting the folate receptor in the treatment/imaging of cancers. *Chem Sci.* **2018**;9(4):790–810. doi:10.1039/C7SC04004K
30. Cheung A, Opzoomer J, Ilieva KM, et al. Anti-folate receptor alpha-directed antibody therapies restrict the growth of triple-negative breast cancer. *Clin Cancer Res.* **2018**;24(20):5098–5111. doi:10.1158/1078-0432.CCR-18-0652
31. Necas D, Klapetek P. Gwyddion: an open-source software for SPM data analysis. *Cent Eur J Phys.* **2012**;10(1):181–188.
32. Crich SG, Cadenazzi M, Lanzardo S, et al. Targeting ferritin receptors for the selective delivery of imaging and therapeutic agents to breast cancer cells. *Nanoscale.* **2015**;7(15):6527–6533. doi:10.1039/C5NR00352K
33. Jiang B, Fang L, Wu KM, Yan XY, Fan KL. Ferritins as natural and artificial nanozymes for theranostics. *Theranostics.* **2020**;10(2):687–706. doi:10.7150/thno.39827
34. Yao HC, Long XF, Cao L, et al. Multifunctional ferritin nanocages for bimodal imaging and targeted delivery of doxorubicin into cancer cells. *RSC Adv.* **2016**;6(111):109322–109333. doi:10.1039/C6RA13845D
35. Stuhn L, Auernhammer J, Dietz C. pH-dependent protein shell dis- and reassembly of ferritin nanoparticles revealed by atomic force microscopy. *Sci Rep.* **2019**;9:1–9. doi:10.1038/s41598-019-53943-3
36. Yang R, Gao YJ, Zhou ZK, Strappe P, Blanchard C. Fabrication and characterization of ferritin-chitosan-lutein shell-core nanocomposites and lutein stability and release evaluation in vitro. *RSC Adv.* **2016**;6(42):35267–35279. doi:10.1039/C6RA04058F
37. Zang JC, Chen H, Zhao GH, Wang FD, Ren FZ. Ferritin cage for encapsulation and delivery of bioactive nutrients: from structure, property to applications. *Crit Rev Food Sci Nutr.* **2017**;57(17):3673–3683. doi:10.1080/10408398.2016.1149690
38. Takahashi T, Kuyucak S. Functional properties of threefold and fourfold channels in ferritin deduced from electrostatic calculations. *Biophys J.* **2003**;84(4):2256–2263. doi:10.1016/S0006-3495(03)75031-0
39. Bazak R, Houri M, El Achy S, Kamel S, Refaat T. Cancer active targeting by nanoparticles: a comprehensive review of literature. *J Cancer Res Clin Oncol.* **2015**;141(5):769–784. doi:10.1007/s00432-014-1767-3
40. Stella B, Arpicco S, Peracchia MT, et al. Design of folic acid-conjugated nanoparticles for drug targeting. *J Pharm Sci.* **2000**;89(11):1452–1464. doi:10.1002/1520-6017(200011)89:11<1452::AID-JPS8>3.0.CO;2-P
41. De Jong WH, Borm PJA. Drug delivery and nanoparticles: applications and hazards. *Int J Nanomed.* **2008**;3(2):133–149. doi:10.2147/IJN.S596
42. Kim M, Rho Y, Jin KS, et al. pH-dependent structures of ferritin and apoferritin in solution: disassembly and reassembly. *Biomacromolecules.* **2011**;12(5):1629–1640. doi:10.1021/bm200026v
43. Reif GA, Wallace DP. ADPKD cell proliferation and Cl<sup>-</sup>-dependent fluid secretion. In: Weimbs T, editor. *Methods in Cell Biology.* Vol. 153. Academic Press; **2019**:69–92.
44. de la Harpe KM, Kondiah PPD, Choonara YE, Marimuthu T, Du Toit LC, Pillay V. The hemocompatibility of nanoparticles: a review of cell-nanoparticle interactions and hemostasis. *Cells.* **2019**;8(10):1–25. doi:10.3390/cells8101209
45. Salvati A, Pitek AS, Monopoli MP, et al. Transferrin-functionalized nanoparticles lose their targeting capabilities when a biomolecule corona adsorbs on the surface. *Nat Nanotechnol.* **2013**;8(2):137–143. doi:10.1038/nnano.2012.237
46. Al-Salama ZT, Syed YY, Scott LJ. Lenvatinib: a review in hepatocellular carcinoma. *Drugs.* **2019**;79(6):665–674. doi:10.1007/s40265-019-01116-x
47. Colombo C, De Leo S, Di Stefano M, Vannucchi G, Persani L, Fugazzola L. Primary adrenal insufficiency during lenvatinib or vandetanib and improvement of fatigue after cortisone acetate therapy. *J Clin Endocrinol Metab.* **2019**;104(3):779–784. doi:10.1210/je.2018-01836
48. Zhang C, Zhang A, Hou W, et al. Mimicking pathogenic invasion with the complexes of Au22(SG)18-engineered assemblies and folic acid. *ACS Nano.* **2018**;12(5):4408–4418. doi:10.1021/acsnano.8b00196
49. Hogemann-Savellano D, Bos E, Blondet C, et al. The transferrin receptor: a potential molecular imaging marker for human cancer. *Neoplasia.* **2003**;5(6):495–506. doi:10.1016/S1476-5586(03)80034-9
50. Rho JK, Choi YJ, Lee JK, et al. The role of MET activation in determining the sensitivity to epidermal growth factor receptor tyrosine kinase inhibitors. *Mol Cancer Res.* **2009**;7(10):1736–1743. doi:10.1158/1541-7786.MCR-08-0504
51. Yang J, Chen H, Vlahov IR, Cheng JX, Low PS. Evaluation of disulfide reduction during receptor-mediated endocytosis by using FRET imaging. *Proc Natl Acad Sci U S A.* **2006**;103(37):13872–13877. doi:10.1073/pnas.0601455103
52. Low PS, Kularatne SA. Folate-targeted therapeutic and imaging agents for cancer. *Curr Opin Chem Biol.* **2009**;13(3):256–262. doi:10.1016/j.cbpa.2009.03.022
53. Yang J, Chen HT, Vlahov IR, Cheng JX, Low PS. Characterization of the pH of folate receptor-containing endosomes and the rate of hydrolysis of internalized acid-labile folate-drug conjugates. *J Pharmacol Exp Ther.* **2007**;321(2):462–468. doi:10.1124/jpet.106.117648
54. Kidane TZ, Sauble E, Linder MC. Release of iron from ferritin requires lysosomal activity. *Am J Physiol Cell Physiol.* **2006**;291(3):445–455. doi:10.1152/ajpcell.00505.2005
55. Kwok JC, Richardson DR. Examination of the mechanism(s) involved in doxorubicin-mediated iron accumulation in ferritin: studies using metabolic inhibitors, protein synthesis inhibitors, and lysosomotropic agents. *Mol Pharmacol.* **2004**;65(1):181–195. doi:10.1124/mol.65.1.181
56. Li WJ, Croce K, Steensma DP, McDermott DF, Ben-Yehuda O, Moslehi J. Vascular and metabolic implications of novel targeted cancer therapies focus on kinase inhibitors. *J Am Coll Cardiol.* **2015**;66(10):1160–1178. doi:10.1016/j.jacc.2015.07.025
57. Carlomagno F, Vitagliano D, Guida T, et al. ZD6474, an orally available inhibitor of KDR tyrosine kinase activity, efficiently blocks oncogenic RET kinases. *Cancer Res.* **2002**;62(24):7284–7290.
58. Jeong Y, Bae SY, You D, et al. EGFR is a therapeutic target in hormone receptor-positive breast cancer. *Cell Physiol Biochem.* **2019**;53(5):805–819.
59. Mechera R, Soysal SD, Piscuoglio S, et al. Expression of RET is associated with Oestrogen receptor expression but lacks prognostic significance in breast cancer. *BMC Cancer.* **2019**;19:1–10. doi:10.1186/s12885-018-5262-0
60. Matsui J, Funahashi Y, Uenaka T, Watanabe T, Tsuruoka A, Asada M. Multi-kinase inhibitor E7080 suppresses lymph node and lung metastases of human mammary breast tumor MDA-MB-231 via inhibition of vascular endothelial growth factor-receptor (VEGF-R) 2 and VEGF-R3 kinase. *Clin Cancer Res.* **2008**;14(17):5459–5465. doi:10.1158/1078-0432.CCR-07-5270
61. Nasir A, Holzer TR, Chen M, Man MZ, Schade AE. Differential expression of VEGFR2 protein in HER2 positive primary human breast cancer: potential relevance to anti-angiogenic therapies. *Cancer Cell Int.* **2017**;17:1–12. doi:10.1186/s12935-017-0427-5
62. Goussia A, Simou N, Zagouri F, et al. Associations of angiogenesis-related proteins with specific prognostic factors, breast cancer subtypes and survival outcome in early-stage breast cancer patients. A hellenic cooperative oncology group (HeCOG) trial. *PLoS One.* **2018**;13(7):1–19. doi:10.1371/journal.pone.0200302

**International Journal of Nanomedicine****Dovepress****Publish your work in this journal**

The International Journal of Nanomedicine is an international, peer-reviewed journal focusing on the application of nanotechnology in diagnostics, therapeutics, and drug delivery systems throughout the biomedical field. This journal is indexed on PubMed Central, MedLine, CAS, SciSearch®, Current Contents®/Clinical Medicine,

Journal Citation Reports/Science Edition, EMBase, Scopus and the Elsevier Bibliographic databases. The manuscript management system is completely online and includes a very quick and fair peer-review system, which is all easy to use. Visit <http://www.dovepress.com/testimonials.php> to read real quotes from published authors.

Submit your manuscript here: <https://www.dovepress.com/international-journal-of-nanomedicine-journal>